THE JOURNAL OF BIOLOGICAL CHEMISTRY
Vol. 278, No. 3, Issue of January 17, pp. 2008–2014, 2003
Printed in U.S.A.

Observation of an Arsenic Adduct in an Acetyl Esterase Crystal Structure*

Received for publication, October 2, 2002
Published, JBC Papers in Press, November 5, 2002, DOI 10.1074/jbc.M210103200

Xueyong Zhu‡§, Nicholas A. Larsen‡, Amrik Basran¶, Neil C. Bruce¶, and Ian A. Wilson‡§‖

From the ‡Department of Molecular Biology and §The Skaggs Institute for Chemical Biology, The Scripps Research Institute, La Jolla, California, 92037 and ¶Center for Novel Agricultural Products, Department of Biology (Area 8), University of York, P. O. Box 373, York YO10 5YW, United Kingdom

The crystal structures of an acetyl esterase, HerE, and its complex with an inhibitor dimethylarsinic acid have been determined at 1.30- and 1.45-Å resolution, respectively. Although the natural substrate for the enzyme is unknown, HerE hydrolyzes the acetyl groups from heroin to yield morphine and from phenyl acetate to yield phenol. Recently, the activity of the enzyme toward heroin has been exploited to develop a heroin biosensor, which affords higher sensitivity than other currently available detection methods. The crystal structure reveals a single domain with the canonical α/β hydrolase fold with an acyl binding pocket that snugly accommodates the acetyl substituent of the substrate and three backbone amides that form a tripartite oxyanion hole. In addition, a covalent adduct was observed between the active site serine and dimethylarsinic acid, which inhibits the enzyme. This crystal structure provides the first example of an As-containing compound in a serine esterase active site and the first example of covalent modification of serine by arsenic. Thus, the HerE complex reveals the structural basis for the broad scope inhibition of serine hydrolases by As(V)-containing organic compounds.

Heroin (3,6-diacetylmorphine) is a highly addictive, synthetic derivative of the alkaloid morphine (Fig. 1*A*). The instability of the 3-acetyl suggests that it can undergo rapid spontaneous hydrolysis to give 6-acetylmorphine. HerE is known to hydrolyze the 6-acetyl of 6-acetylmorphine to yield morphine (k_{cat} = 12.6 ± 0.6 s^{-1}, K_m = 0.5 ± 0.06 mM) and was originally identified from the *Rhodococcus* sp. strain H1 by selective growth using heroin as the sole carbon source (1). Identification of this esterase has facilitated development of a coupled enzyme biosensor for heroin detection (Fig. 1*A*) with higher sensitivity than other currently available technology (2). In brief, hydrolysis of heroin by HerE generates morphine, which is the substrate for NADPH-dependent morphine dehydrogenase. The activity of morphine dehydrogenase is directly monitored by bacterial luciferase, which outputs a bioluminescent signal at 490 nm (Fig. 1*A*) (2). The higher activity (k_{cat} K_m^{-1}) of HerE toward smaller substrates such as phenyl acetate (Fig. 1*B*) (k_{cat} = 3.0 ± 0.05 s^{-1}, K_m = 70 ± 8 nM at pH = 6.4) provides a benchmark for engineering the esterase binding pocket to accept bulkier substrates more efficiently. Hence, the crystal structure of this acetyl esterase should provide substantial insights for structure-based design of second generation heroin biosensors with improved sensitivity.

In addition, our structure with the inhibitor dimethylarsinic acid (Fig. 1*B*) demonstrates for the first time the covalent modification of serine by arsenic. Arsenic lies directly below phosphorous in the periodic table and shares some similar properties, but in general, arsenic is more reactive. As(V)-containing organic compounds comprise a known class of broad scope serine esterase/protease inhibitors (3, 4). Usually, arsonic R-As(V)O_3H_2 and arsinic R_2-As(V)O_2H compounds have K_i values in the μM-mM range (3, 4), but surprisingly, the mechanistic basis for inhibition of esterase/proteases by As(V) compounds has never been defined from a crystal structure. The HerE esterase is the ideal model system for studying inhibition by dimethylarsinic acid, since the methyl groups correspond to the acetyl moiety that is hydrolyzed from heroin and phenyl acetate (Fig. 1*C*).

The most common form of inorganic arsenic is As(V)O_4^{3-} (arsenate), which is reduced by As(V) reductases *in vivo* to As(III)O_3^{3-} (arsenite). Interestingly, arsenite is further metabolized to several methylated species, CH_3As(V)O_3^{2-}, CH_3As(III)O_2^{2-}, $(CH_3)_2$As(V)O_2^- (cacodylate or dimethylarsinic acid), and $(CH_3)_2$As(III)O^-, which are less cytotoxic than the inorganic form but may have a longer term carcinogenic impact in chronic exposure (5). These As(III) arsenicals are generally regarded as the more reactive and most toxic species (5), and crystal structures in the Protein Data Bank confirm that As(III) compounds form covalent adducts with cysteine (6). Our HerE crystal structure now demonstrates that dimethylarsinic acid, one of the key metabolites associated with chronic arsenic toxicity, could also form a covalent adduct with a reactive serine in a catalytic triad at sufficiently high concentrations.

EXPERIMENTAL PROCEDURES

Cloning, Expression, and Crystallization—The HerE enzyme was subcloned into pET-28a(+) (Novagen) (7) and transformed into BL21-Gold (DE3) cells (Stratagene). Soluble native enzyme (60 mg $liter^{-1}$ Luria broth) was obtained by overnight induction with 1 mM isopropyl-1-thio-β-D-galactopyranoside at ~23 °C and was ~99% pure after 2 consecutive rounds of nickel nitrilotriacetic acid-agarose chromatography (Qiagen). The amino-terminal His tag was removed by overnight thrombin digestion at 4 °C, and the enzyme was further purified by ion exchange chromatography with a MonoQ column (Amersham Biosciences). Subsequently, HerE was dialyzed into 20 mM Tris, pH 7.5, 25 mM NaCl and concentrated to 15 mg ml^{-1} for crystallization trials. Selenomethionine derivative enzyme was made and purified similarly

* The work was supported by National Institutes of Health Grant GM38273 (to I. A. W.) and the Biotechnology and Biological Sciences Research Council (to N. C. B.). The costs of publication of this article were defrayed in part by the payment of page charges. This article must therefore be hereby marked "*advertisement*" in accordance with 18 U.S.C. Section 1734 solely to indicate this fact.

The atomic coordinates and structure factors (code 1LZL and 1LZK) have been deposited in the Protein Data Bank, Research Collaboratory for Structural Bioinformatics, Rutgers University, New Brunswick, NJ (http://www.rcsb.org/).

‖ To whom correspondence should be addressed: Dept. of Molecular Biology, The Scripps Research Institute, 10550 North Torrey Pines Rd. BCC206, La Jolla, CA, 92037. Tel.: 858-784-9706; Fax: 858-784-2980; E-mail: wilson@scripps.edu.

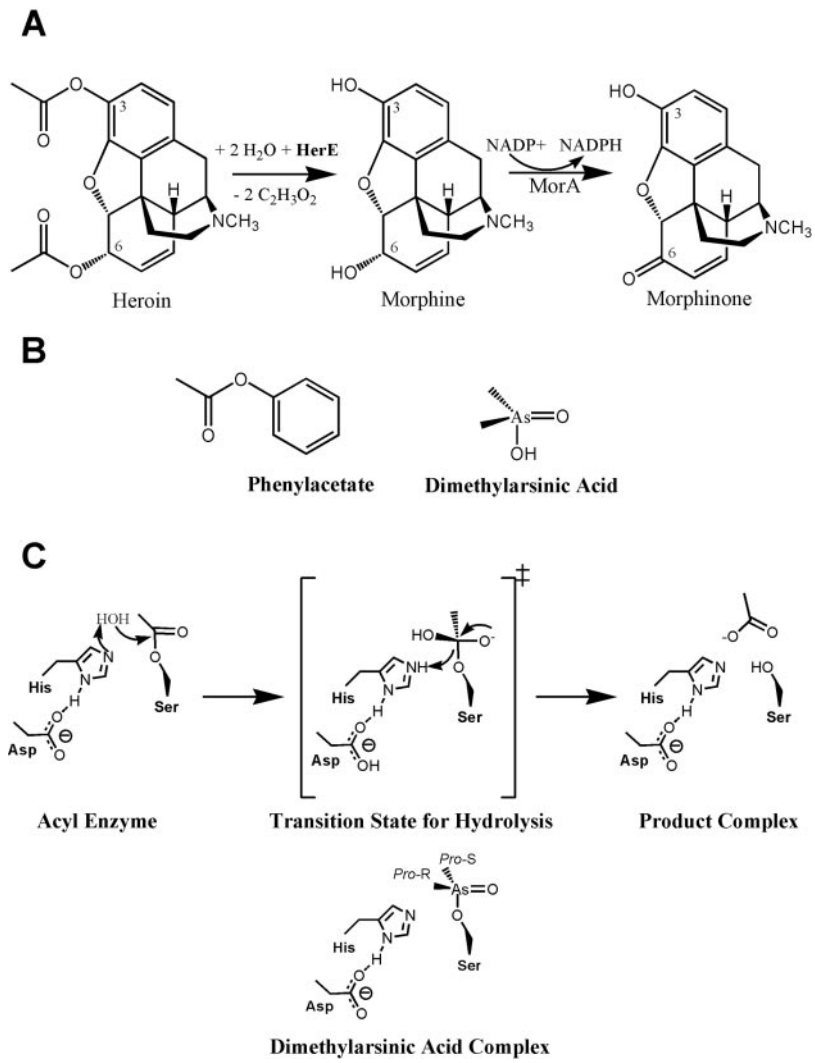

FIG. 1. **Substrates and mechanism for arsenic inhibition.** *A*, schematic for heroin biosensor. The 3-acetyl ester of heroin undergoes rapid spontaneous hydrolysis, whereas the 6-acetyl ester is hydrolyzed by acetyl esterase (*HerE*) to give morphine. Morphine dehydrogenase (*MorA*) oxidizes the alcohol to the ketone in an NADPH-dependent reaction. The reduction of $NADP^+$ to NADPH is monitored directly by bacterial luciferase, which outputs a signal at 490 nm. *B*, structures of substrate phenyl acetate and inhibitor dimethylarsinic acid. *C*, hydrolysis of the acyl enzyme intermediate. Hydrolysis of both heroin and phenyl acetate yields the common acyl enzyme intermediate. Hence, the complex with dimethylarsinic acid resembles the transition state for hydrolysis of the acyl enzyme for both substrates investigated.

from the methionine auxotroph strain B834-(DE3) grown in minimal media substituted with 0.3 mM selenomethionine (Sigma). The selenomethionine enzyme was concentrated to 6–7 mg ml^{-1} for crystallization in the same protein buffer. The arsenic adduct, selenium-derivative crystals, were grown in 1.8 M ammonium sulfate, 0.1 M NaCl, 0.1 M cacodylate, pH 6.5, and native crystals were grown in 1.7 M ammonium sulfate, 0.1 M NaCl, 0.1 M BES[1] buffer, pH 6.4.

Gel Filtration, Biochemical Activity, and Arsenic Inhibition—The apparent native molecular weight of the esterase was determined using gel filtration chromatography on a Superdex 200 10/30 HR column calibrated with low and high molecular weight protein standards (Amersham Biosciences). A calibration curve was constructed from a plot of log molecular weight of the standard *versus* K_{av}. Purified esterase (50 μg) was applied to the column at a linear flow rate of 0.25 ml min^{-1}, and the elution volume was determined by monitoring absorption at 280 nm.

Enzyme concentrations were determined using the Coomassie Plus protein assay reagent kit (Pierce) with bovine serum albumin as the standard. Steady state kinetic measurements for 6-acetylmorphine were measured at 294 nm in the presence of 10 μg of protein in 100 mM sodium phosphate buffer, pH 8.0, at 25 °C with a Hewlett-Packard 8452A single beam diode array spectrophotometer. A molar extinction coefficient of $\epsilon = 1050\ M^{-1}\ cm^{-1}$ at 294 nm was used to determine the concentration of product formed during the reaction. K_m and k_{cat} values were determined by varying the concentration of 6-acetylmorphine and fitting the data to the Michaelis-Menten equation using the Grafit 4 software package (Erithacus Software Ltd, Staines, UK). Inhibition measurements for dimethylarsinic acid were performed using phenyl acetate as a model substrate in conditions designed to mimic the crystallization conditions as closely as possible. The molar extinction coefficient E_{270} for phenol was determined from a standard curve to be $856.8\ M^{-1}\ cm^{-1}$. The reaction was initiated by adding 150 μl of a 2× substrate solution to 150 μl of a 2× enzyme solution in a 96-well UV plate (Costar). Steady state kinetics were monitored at 270 nm in the presence of 0.25 $\mu g\ ml^{-1}$ protein in 50 mM BES buffer, pH 6.4 (uninhibited reaction), and 100 and 50 mM cacodylate buffer, pH 6.4 (inhibited reaction), at room temperature with a SpectraMax Plus 384 UV plate reader (Molecular Devices). K_m, $K_{M\,app}$, and k_{cat} values were determined by varying the concentration of phenyl acetate in serial dilutions (50 μM–100 nM) and fitting the data to the Michaelis-Menten equation using Kaleidagraph V 3.5 (Abelbeck Software).

Data Collection, Structure Solution, and Refinement—A single wavelength anomalous diffraction (SAD) data set was collected at Stanford Synchrotron Radiation Laboratory (SSRL) beamline 11–1 from a selenomethionine derivative crystal at a high energy remote wavelength, and a native data set was collected at SSRL beamline 9–2 (Table I). The space group is $P3_221$ with $a = b = 71.4$ Å, $c = 105.7$ Å (native), and $a = b = 71.6$ Å, $c = 106.2$ Å (complex), with one molecule per asymmetric unit and a Matthews coefficient of 2.1 $Å^3\ Da^{-1}$ (solvent content of ~42%). The data were integrated and scaled with HKL2000 (8), and two selenium sites and one arsenic site were found using the program SOLVE (9), which was sufficient to phase the data at 2.0 Å (figure of merit = 0.36, all reflections). Density modification was performed using RESOLVE (figure of merit = 0.61, all reflections) (10), and the selenomethionine derivative phases were extended to 1.45 Å using Arp/Warp (11). Arp/Warp then successfully traced and built ~80% of the structure (11). The remaining model was built manually in O (12), and the refinement was started in CNS (13) and finished using SHELXL (14) with final $R_{cryst} = 15.7\%$ and $R_{free} = 22.3\%$ for all data. The native structure was refined using the SAD structure as a starting model with the final $R_{cryst} = 15.3\%$, and $R_{free} = 21.3\%$.

[1] The abbreviations used are: 2- BES, [bis(2-hydroxyethyl)amino]ethanesulfonic acid; SAD, single wavelength anomalous diffraction.

TABLE I
Data collection and refinement statistics

r.m.s.d., root mean square deviation.

	Native	Se remote (As adduct complex)
Data collection		
Wavelength (Å)	0.94641	0.89471
Resolution range (Å)[a]	26.7–1.30 (1.32–1.30)[a]	24.4–1.45 (1.48–1.45)[a]
Unique reflections	76,984	56,480
Completeness (%)	99.7 (99.5)[a]	99.9 (100)[a]
Redundancy	4.0	21.3
R_{merge} (%)[b]	4.2 (58.5)[a]	7.8 (65.3)[a]
I/σ[b]	35.2 (2.4)[a]	42.2 (3.7)[a]
Refinement statistics		
Refined residues	317	317
Refined waters	313	309
R_{cryst} (%)[c]	15.3 (14.3 $F_o > 4\sigma$)	15.7 (15.0 $F_o > 4\sigma$)
R_{free} (%)[d]	21.3 (20.0 $F_o > 4\sigma$)	22.3 (21.2 $F_o > 4\sigma$)
Average B values (Å^2)		
Enzyme	20.5	20.4
Waters	31.1	34.8
Ligand		13.8
Ramachandran statistics (%)		
Most favored	91.2	88.5
Additional allowed	7.3	9.9
Generously allowed	1.1	1.1
Disallowed[e]	0.4	0.5
Deviations from ideal geometry (r.m.s.d.)		
Bond lengths (Å)	0.011	0.013
Bond angles (°)	2.21	2.26

[a] Numbers in parenthesis refer to the highest resolution shell.
[b] $R_{merge} = [\Sigma_h\Sigma_i|I_i(h) - \langle I(h)\rangle|/\Sigma_h\Sigma_i I_i(h)] \times 100$, where $\langle I(h)\rangle$ is the average intensity of i symmetry-related observations of reflections with Bragg index h.
[c] $R_{cryst} = [\Sigma_{hkl}|F_o - F_c|/\Sigma_{hkl}|F_o|] \times 100$, where F_o and F_c are the observed and calculated structure factors.
[d] R_{free} was calculated as for R_{cryst}, but on 5% of data excluded before refinement.
[e] The disallowed residue, Leu-208, is located in a γ-turn.

RESULTS

General Overview of the Structure—The crystal structure of HerE was determined by SAD from a high energy remote wavelength (Table I). The native enzyme and cacodylate complex were determined at 1.30 and 1.45 Å, and refinement converged to a final R_{cryst} = 15.3%, R_{free} = 21.3% and R_{cryst} = 15.7%, R_{free} = 22.3%, respectively. The enzyme consists of 323 residues with a molecular weight of ~35,000 (GenBank™ accession number U70619). In each structure, residues 1–317 were modeled in the electron density. The globular structure has approximate dimensions of ~35 Å × ~45 Å × ~50 Å, and the overall secondary structure is a mixture of β-sheet (15%) and α-helix (36%) (Fig. 2, *A* and *B*). The enzyme is related to the hormone-sensitive lipase subfamily of enzymes, sharing ~30% sequence identity with related structures, brefeldin A esterase (15), esterase 2 (16), and *Archaecoglobus fulgidus* esterase (17). In brief, HerE has a single domain with the canonical α/β hydrolase fold, which typifies esterases with a Ser/Cys-Asp/Glu-His catalytic triad. The fold consists of repeating β-α-β motifs that form a central, predominantly parallel (except β2) eight-stranded β-sheet (strand order β1, β2, β4, β3, β5, β6, β7, β8) surrounded on either side by α-helices (Fig. 2, *A* and *B*). The core β-sheet and the β-α-β motifs are all right-handed, except for the unusual left-handed junction between strand β8 and helix F′, which is necessary to properly position the catalytic histidine residue in the active site (18). In the hydrolase family of enzymes, insertions are commonly observed in the canonical structure at the amino and carboxyl termini and at the junction between strands β6 and β7. Such insertions are believed to modulate the substrate specificity of the enzyme (18, 19). HerE has two predominantly helical, ~50-amino acid insertions, one at the amino terminus (H1, H2) and the other (H3, H4) between strands β6 and β7 (Fig. 2, *A* and *B*).

Crystal Packing Supports a Dimer Model—Analysis of the packing within the crystal shows that HerE forms a dimer,

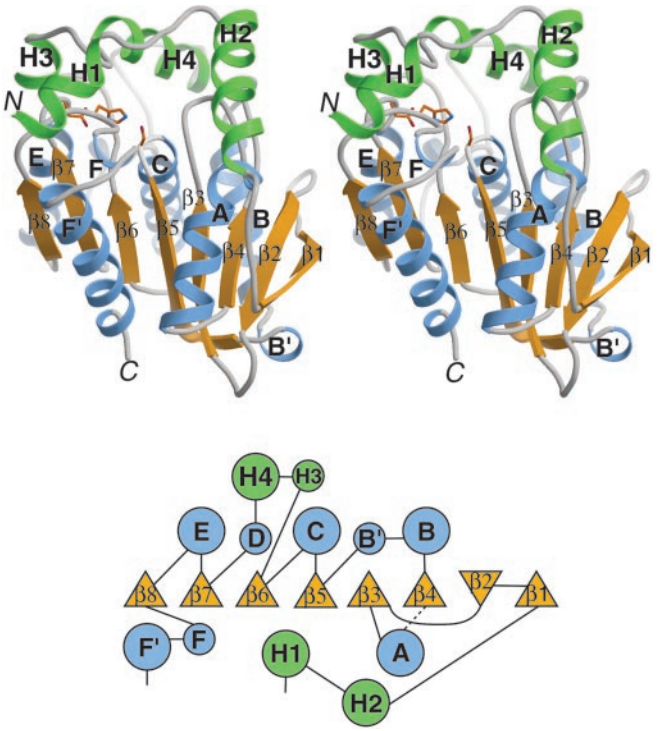

FIG. 2. **Overall structure of HerE.** *A*, the stereo diagram of HerE reveals the canonical α/β hydrolase fold. The β-sheet and α-helices of the canonical α/β hydrolase fold are colored *orange* and *blue*, whereas the insertions at the amino terminus and between β6 and β7 are colored *green*. This coloring scheme will be adopted in all subsequent figures. The catalytic triad (*ball* and *stick*) is shown in the active site. The figure was produced in Bobscript (33) and rendered in Raster3D (34). *B*, topology diagram of HerE (35). The *triangles* represent β-strands, and the *circles* represent α-helices. The directionality of each β-strand is indicated by the orientation of the *triangle*.

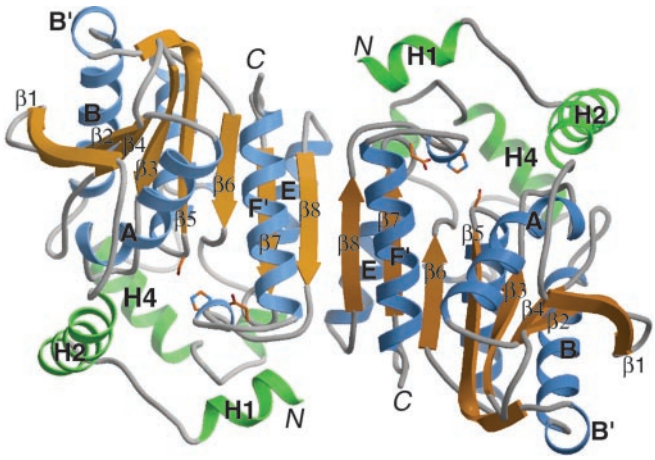

FIG. 3. **HerE forms a dimer.** In this view, the two molecules are rendered in *light* and *dark shades* and are related by a 2-fold crystallographic axis that is perpendicular to the plane of the paper. The interface is formed by continuation of the central β-sheet via four hydrogen bonds between strands β8. In addition, there are coiled-coil interactions between helices E-E and F′-F′.

where each monomer is related to the other by a crystallographic 2-fold (Fig. 3). In the dimer interface, strands β8 from each monomer align antiparallel to each other to form four backbone hydrogen bonds so that the β-sheet from one monomer is continuous with the β-sheet of the other. In addition, helices αE and αF′ from each monomer form coiled-coil motifs, αE-αE and αF′-αF′ at the interface. In total, the dimer interface buries 1890 Å^2 (20) and forms 144 van der Waals contacts, 11 hydrogen bonds, and 8 salt bridges (21). In comparison, the V_H/V_L interface of a Fab typically buries 1000–1400 Å^2 (22), and hence, the HerE dimer is likely to be relatively stable in solution. Determination of the native molecular weight by high resolution gel filtration chromatography supports this model of a stable dimer with an apparent molecular mass of 73 ± 4 kDa. This mode of dimerization is similar to that seen in other members of the hormone-sensitive lipase subfamily (15).

Identification of Arsenic in the Active Site—Crystals grown in 50 mM cacodylate buffer (dimethylarsinic acid) yielded a tetrahedral covalent adduct between the Ser-160 Oγ and arsenic (Fig. 4, *A* and *B*). Arsenic was unequivocally identified as the heavy atom from an x-ray fluorescence scan, an anomalous difference map calculated with data collected at the arsenic absorption peak (λ = 1.0439 Å), and comparison to native crystals grown in the absence of cacodylate buffer. From this arsenic adduct, the prototypic catalytic triad was identified as Ser-160, Asp-260, and His-290 at the carboxyl end of strands β5, β7, and β8, respectively. Ser-160 (ϕ = 55°, ψ = −121°) is located in the so-called nucleophilic elbow within the conserved GX_1SX_2G motif (GQSAG), a signature sequence for the hydrolase family (18). In the arsenic adduct, the divalent oxygen is in a tridentate oxyanion hole, where it could form hydrogen bonds with the backbone amides of Ala-161, Gly-88, and Gly-89, located between strand β3 and helix αA (Fig. 4*B*). Two rotamers of the nucleophilic Ser-160 were refined in both the native structure (Fig. 4*A*) and the As complex (Fig. 4*B*), with arsenic bound to only one of the possible conformers. The occupancy of arsenic, therefore, was refined and found to be 0.61, which implies a mixture of bound and unbound species within the crystal.

The Acyl and Alcohol Specificity Pockets—The dimethylarsinic acid adduct is 91% buried (20) and forms 32 van der Waals contacts (21) in the active site. The pro-*S* methyl group corresponds to the methyl group of the heroin acetyl ester that is hydrolyzed by HerE (Figs. 1 and 4*B*). This methyl sits snugly inside the acyl binding pocket (Fig. 4*B*) and suggests that the enzyme may preferentially hydrolyze small acyl groups (three carbons or less) from esters. The pro-*S* methyl abuts the π-face of Trp-209, forming nine favorable van der Waals contacts. In addition, Glu-190 is buried at the back of the acyl binding pocket, forming hydrogen bonds with Ser-217 and a water molecule. The presence of the charged residue is unexpected given the neutrality of the acyl ester and differs from the acyl binding pocket of acetylcholinesterase, which is entirely hydrophobic (23). The electronegative potential in HerE may facilitate expulsion of the negatively charged product, acetate, as part of an evolved negative design strategy to avoid product inhibition. Alternatively, the negative charge may be important for modulating the specificity of the enzyme for other as yet unidentified substrates.

The putative alcohol binding pocket is fairly wide compared with the 6-acetylmorphine substrate. Therefore, it is possible to model morphine in several different orientations, which taken together implicate hypothetical interactions with Val-21, Phe-23, Tyr-33, Ile-92, Gln-159, Leu-208, and Leu-294. Based on this modeling alone, we speculate possible hydrogen bonding between the morphine nitrogen and the side chains of either Gln-159 or Tyr-33 but defer definitive characterization until a complex with morphine becomes available. Leu-208 (ϕ = 72°, ψ = −53°) is located at the apex of a γ-turn, which may be important in positioning Trp-209 in the acyl binding pocket. The amino-terminal insertion contributes many of the residues that line this putative alcohol binding pocket. This insertion has an average isotropic B value of ~38 Å^2 compared with only ~17 Å^2 for the rest of the protein, and portions of this domain are relatively disordered in the electron density. These elevated B values suggest inherent flexibility in this part of the molecule that may be of relevance for substrate recognition.

Geometry of the Arsenic Adduct—Our structure demonstrates that As(V)-containing organic arsenicals react specifically with serine, forming an adduct that resembles the tetrahedral transition state for deacylation (Fig. 4*B*). Although the electron density shows the arsenic is coordinated by four ligands (two methyl groups, the Ser-163 Oγ, and divalent oxygen), the bond angles are distorted from the expected tetrahedral geometry seen in small molecule crystal structures of cacodylate. This deviation from ideal geometry may indicate considerable strain or chemical reactivity within the enzyme inhibitor complex.

In the refined complex, the bond lengths of As to Ser-Oγ is 1.98 Å, from As to divalent oxygen is 1.59 Å, and from As to the methyl groups is 1.82 Å (pro-*S*) and 1.88 Å (pro-*R*). These bond lengths are within the range of possible values for arsenate compounds surveyed in the small molecule Cambridge Structural Database (24). Importantly, these refined values show that the oxygen is divalent, and As is in the plus five oxidation state. The bond angles of the arsenic adduct reveal additional strain from classic tetrahedral geometry seen in covalent adducts with phosphonate transition state analogs (25, 26). In fact, the bond angles suggest the configuration of the arsenic ligands in some respects is closer to trigonal bipyramidal than tetrahedral geometry. For example, the Ser-160 Oγ is apparently in an apical position as the bond angles are 90.2° (Oγ-As-pro-*S* CH_3), 108.2° (Oγ-As-pro-*R* CH_3), and 95.3° (Oγ-As═O). In addition, the arsenic ligands CH_3 (pro-*R* and -*S*) and divalent oxygen are nearly coplanar and are separated by 115.3° (pro-*S* CH_3-As═O), 116.5° (pro-*R* CH_3-As═O), and 122.2° (CH_3-As-CH_3) (Fig. 4*B*). These values differ from the ideal tetrahedral bond angles seen in the small molecule crystal structure of cacodylate. Considerable strain should be expected

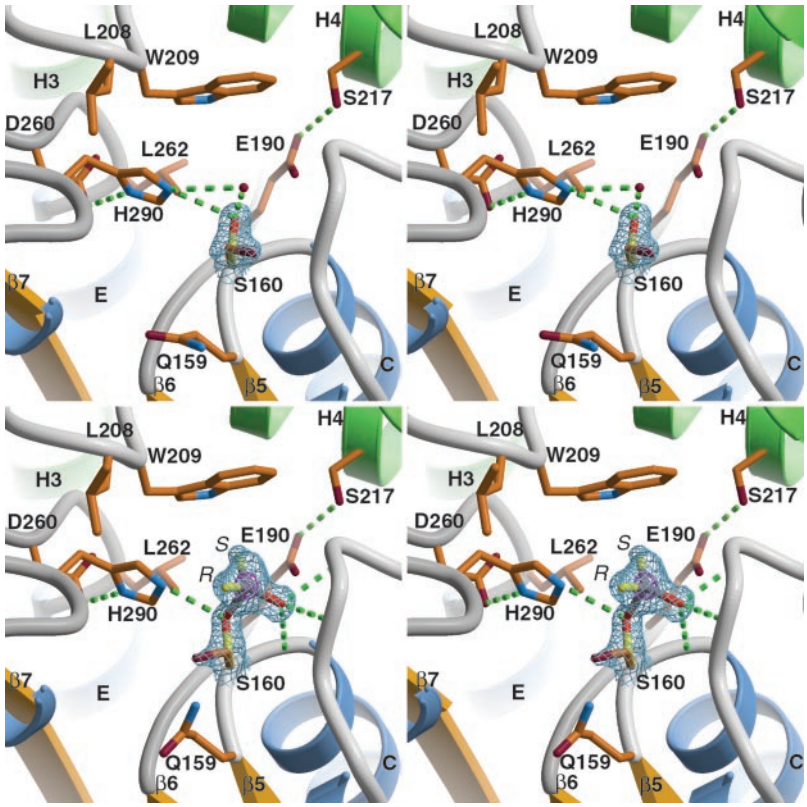

FIG. 4. **Stereo views of the HerE active site.** Ser-160 has alternate conformations in both the native and complex structures. The rotamer with the higher occupancy is indicated in *yellow*, and that of the lesser is indicated in *brown*. *A*, the native structure. The water molecule HOH (*red sphere*) nearly superimposes on the pro-*R* methyl substituent of the arsenic complex. The hydrogen bond interaction between this water and His-290 suggests that a similarly positioned water could be responsible for nucleophilic attack of the acyl intermediate. The σ_A-weighted $2F_o - F_c$ map is contoured at a 1.3 σ level. *B*, the arsenic complex. Although arsenic is apparently coordinated by only four ligands, the electron density and refined bond angles deviate from classic tetrahedral geometry and are close to a trigonal bipyramidal geometry. The enzyme likely imposes this strain, and the observed geometry supports our proposed reaction mechanism that includes a trigonal bipyramidal transition state. The σ_A-weighted $2F_o - F_c$ map is contoured at 1.2 σ (*blue*) and 8.0 σ (*magenta*), precisely centered on the arsenic.

given that the natural transition state of the enzymatic reaction involves carbon, which has a much smaller atomic radius than arsenic (0.91 *versus* 1.33 Å).

Comparison of Native and Complex Structures—The native and complex structures closely superimpose (root mean square deviation = 0.2 Å for all Cα atoms). In both crystal structures, the His-290 Nϵ2 atom is ~3.3 Å from the Ser-160 Oγ, which approaches the upper limit of separation for these two residues in a catalytic triad (Fig. 4, *A* and *B*). His-290 is precisely oriented in this position by close interaction with Asp-260, Leu-208, and Trp-209. In the arsenic complex, the His-290 Nϵ2 is ~3 Å from the pro-*R* methyl and, in the native structure it is ~3.4 Å from a water molecule (Fig. 4, *A* and *B*). This water molecule forms hydrogen bonds with His-290 Nϵ2 and Ser-160 Oγ and would nearly superimpose on the pro-*R* methyl of the arsenic adduct (Fig. 4*A*). Hence, this water molecule would be ideally positioned for activation and subsequent nucleophilic attack of the acyl intermediate. In both structures, alternate conformations were visible for the active site Ser-160. However, the alternative rotamer in the native structure differs from that in the arsenic adduct structure. Multiple conformations for the active site serine may be of importance mechanistically during initial substrate binding or product release. The observation of three serine rotamers is unusual in a catalytic triad (27) and is possibly attributable to the relatively distant interaction with His-290.

Structural Homology with Other Esterases—Three crystal structures are known from the hormone-sensitive lipase subfamily of hydrolases, brefeldin A esterase (15), esterase 2 (16), and *Archaecoglobus fulgidus* esterase (17). The DALI Z score (28) for HerE and brefeldin A esterase was 37, which is exceptionally high (a Z-score > 12 is significant homology). Superposition illustrates that all of these homologous enzymes share similar helical insertions at the amino terminus and between strand β6 and β7, and all of these enzymes exhibit a similar mode of dimerization. Mechanistically, this subfamily employs three backbone amides in the oxyanion hole, similar to scattered reports for several other lipases and acetylcholinesterase, which belong to related esterase subfamilies (16, 29). This tripartite oxyanion hole differs from the classic bipartite oxyanion hole seen in most proteases and esterases (19). The third hydrogen bond in acetylcholinesterase has been invoked to explain, in part, the remarkable diffusion-limiting rate acceleration for this particular enzyme (29).

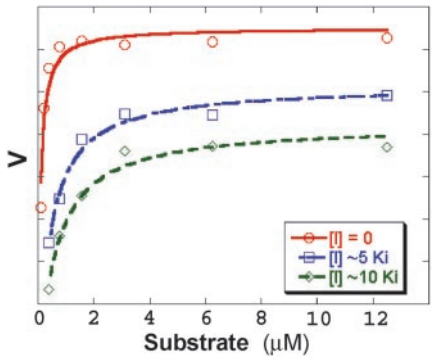

FIG. 5. **Dimethylarsinic acid inhibition.** The K_i for dimethylarsinic acid was determined using phenyl acetate as a model substrate. The uninhibited reaction is shown in *red circles*, and the inhibited reactions are shown in *blue squares* (50 mM cacodylate) and *green diamonds* (100 mM cacodylate). The data have been fit to the Michaelis-Menten equation. For the inhibited reactions, the apparent K_m is a factor of $(1 + [I]\ K_i^{-1})$ greater than the true K_m.

Substrate Specificity in the Active Site—Because the 3-acetyl ester appears to undergo rapid spontaneous hydrolysis, it is impractical to measure Michaelis constants for this substrate. Therefore, the specificity of HerE was determined for two different substrates, 6-acetylmorphine (k_{cat} = 12.6 ± 0.6 s^{-1}, K_m = 500 ± 60 μM) at pH = 8 (data not shown) and phenyl acetate (k_{cat} = 3.0 ± 0.05 s^{-1}, K_m = 70 ± 8 nM) at pH = 6.4 (Fig. 5). The Michaelis constants for phenyl acetate were measured under mildly acidic conditions to directly compare the uninhibited reaction with the inhibited reaction in the cacodylate crystal-

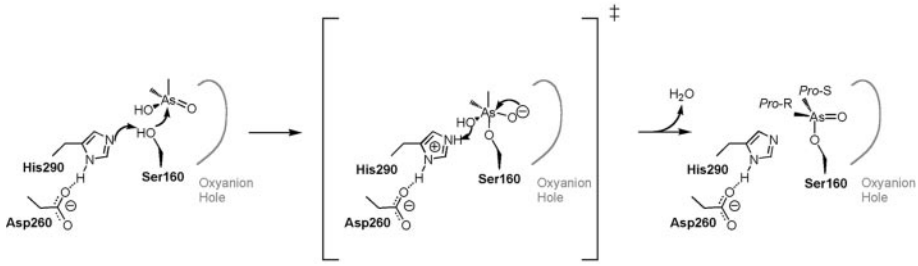

FIG. 6. **Proposed mechanism for arsenic inhibitor binding.** His-290 acts as a general acid and general base. In the first step, His-290 deprotonates the Ser-160 hydroxyl, facilitating nucleophilic attack of arsenic by the reactive serine Oγ. This attack results in the formation of a transient trigonal bipyramidal transition state, where the oxyanion is stabilized by three hydrogen bonds in the oxyanion hole, and the hydroxyl forms a hydrogen bond with His-290. His-290 then acts as a general acid, protonating the hydroxyl leaving group. In the final tetrahedral complex, the oxygen is divalent and remains positioned in the oxyanion hole. The pro-*S* methyl group interacts with Trp-209 in the acyl binding pocket, and the pro-*R* methyl forms close van der Waals contacts with the histidine.

lization buffer, pH = 6.4. The catalytic efficiency of HerE for 6-acetylmorphine ($k_{cat}\ {K_m}^{-1} = 2.5 \times 10^4$ M s^{-1}) is several orders of magnitude less than for phenyl acetate ($k_{cat}\ {K_m}^{-1} = 4.3 \times 10^7$ M s^{-1}) (Fig. 5). The large difference in K_m for the two substrates accounts for the wide variation in efficiency, suggesting that the enzyme is unable to bind heroin as well as phenyl acetate. The high bimolecular rate constant $k_{cat}\ {K_m}^{-1}$ for phenyl acetate at a non-ideal pH 6.4 implies the enzyme would approach the bimolecular diffusion limit ($10^9 - 10^{11}$ M s^{-1}) at a more optimal pH 8, which would be similar to the high efficiency seen for acetylcholinesterase. Further biochemistry within the hormone-sensitive lipase subfamily will illuminate whether or not other members approach a comparable catalytic efficiency as acetylcholinesterase. The structural homology to other lipase enzymes further suggests that HerE may have acylglycerol hydrolytic activity (*e.g.* 1,2,3-triacetylglycerol) (30) and, hence, provides a basis for additional mutagenesis and biochemistry experiments.

Arsenic Inhibition in the Acetyl Esterase—The K_i of dimethylarsinic acid was determined under steady state conditions using phenyl acetate as a model substrate. All reactions were conducted at pH 6.4, which is similar to the pH of the crystallization mother liquor and coincides with the pK_a of cacodylate (Fig. 5). The apparent shift in K_m for phenyl acetate was determined for two different inhibitor concentrations, and the K_i for dimethylarsinic was determined to be ~12 ± 2 mM. The inhibition is most likely competitive, although it was impractical to confirm that V_{max} converges to the same value in the limit of high substrate concentrations. The specific interaction between dimethylarsinic acid and serine in the active site, however, supports this model of competitive inhibition. The relatively high K_i for the inhibitor also suggests that the inhibition is reversible. Based on this K_i value, one would expect that at equilibrium ~80% of the enzyme would be bound in the 50 mM cacodylate crystallization buffer. This value agrees closely with the crystal structure where the refined occupancy of the arsenic adduct was ~60%.

DISCUSSION

Several novel observations have emerged from the crystal structure of HerE. The HerE enzyme is the first structure reported of an esterase known to hydrolyze heroin. Hence, the structure provides a framework for improving the specificity and sensitivity of a recently reported heroin biosensor (2). The high bimolecular rate constant for phenyl acetate (approximately 1000-fold higher than 6-acetylmorphine) implies that with engineering of the active site, the specificity constant for heroin could be substantially improved. Specifically, the structure highlights residues in the acyl and alcohol binding pockets that could be targeted by random and rational mutagenesis to create a binding pocket with higher shape complementarity to morphine. From a more biochemical perspective, truncation of the flexible amino-terminal domain could assess its contribution to activity. These capping domains have been proposed to act as flexible lids in other esterase and lipase structures that regulate access into and out of the active site. In addition, the negatively charged Glu-190 in the acyl binding pockets could be mutated to Gln or Leu to create a binding pocket with higher electrostatic complementarity to heroin.

We also employed unconventional structure determination methodology by using SAD with a high energy remote wavelength rather than the optimal peak wavelength (because of constraints at the beam line). Surprisingly, the anomalous contributions to the structure factors were sufficient for phasing even though the data were not collected at the optimal peak wavelength. The successful structure determination was due, in part, to the high redundancy and quality of the data (Table I) and to the anomalous contributions from both arsenic and selenium. The derivative with arsenic could be applicable to phasing of other esterase/protease structures, since arsenic is a broad scope inhibitor of serine hydrolases (3, 4). Moreover, deposited crystal structures in the Protein Data Bank also demonstrate specific reaction of arsenic with cysteine (6). Hence, arsenic may be generally exploited as a useful heavy metal for either multiple isomorphous replacement (MIR)/single isomorphous replacement (SIR) or multiple wavelength anomalous diffraction (MAD)/single wavelength anomalous diffraction (SAD) phasing.

The acetyl esterase structure is the first to demonstrate reactivity of an As(V)-containing compound in a serine esterase active site and the first example in the Protein Data Bank of covalent modification of serine by arsenic. The apparent dehydration that occurs in the active site is most likely a ligand substitution reaction, where arsenic remains in the As(V) oxidation state throughout. The pK_a of dimethylarsinic acid is ~6.4, so inhibition likely occurs optimally at acidic pH in the protonated form, as an oxyanion is a poor leaving group. Although it is impossible to distinguish between an associative (S_N2-like) or disassociative (S_N1-like) mechanism from the crystal structure alone, we can predict a likely reaction pathway given the geometrical restraints of the active site.

Because hydroxide is also a poor leaving group, the cacodylate hydroxyl must be protonated during the reaction (Fig. 6). Hence, when the Ser-160 nucleophile attacks, the hydroxyl leaving group is likely positioned closest to His-290 for optimal proton transfer in a transient, trigonal bipyramidal-like transition state with Ser-160 Oγ and one of the methyl substituents at the apical positions (Fig. 6). In this transition state, the formerly divalent oxygen becomes monovalent, forming three stabilizing hydrogen bonds in the oxyanion hole, whereas the other methyl substituent points into the

acyl pocket (Fig. 6). Importantly, the trigonal bipyramidal geometry of this proposed transition state is consistent with the apparently strained tetrahedral geometry observed in the adduct structure. In the last step, the monovalent oxyanion collapses to resume divalency, the water molecule is expelled, and the arsenic adduct adopts the strained tetrahedral geometry with the apical methyl group of the transition state, shifting to its pro-*R* position in close contact with His-290. Finally, the proposed mechanism would be fully reversible, which is also consistent with the refined occupancy of 0.61 for the adduct and the relatively high K_i of ~12 mM. Hence, this crystal structure fills a gap in the classic body of literature on catalytic triads (31) and on inhibition of serine hydrolases by arsenic (3, 4).

CONCLUSION

A detailed understanding of this acetyl esterase now gives a foundation for the structure-based iterative design of second generation heroin biosensors with improved sensitivity. Moreover, at least two human carboxylesterases (hCE-1,2) (32) mediate the breakdown of 6-acetylmorphine to morphine, but no structures of these human enzymes have been reported. Hence, HerE provides a glimpse of an active site known to accept heroin as a substrate. The acyl binding pocket is quite small, thus optimally accommodating the acetyl substituent of heroin. It will be interesting to see if this small acyl binding pocket will be a conserved feature of the corresponding human carboxylesterases and whether this pocket could be expanded by site-directed mutagensis to accept larger substrates. Additionally, the active site complex identifies three hydrogen bond interactions in the oxyanion hole, similar to those seen in acetylcholinesterase and several other lipases. Although only a handful of serine hydrolases are known to have three rather than the more common two hydrogen bonds, as more hydrolase structures become available this tripartite oxyanion hole is likely to emerge as a common theme and perhaps provide an alternative rational for categorizing serine hydrolase enzymes.

Our crystal structure also demonstrates, for the first time, covalent modification of the catalytic triad serine by an arsenic compound, dimethylarsinic acid. Arsenic-containing compounds comprise a known class of serine hydrolase inhibitors. Dimethylarsinic acid is of particular interest, because it is a major metabolite formed upon chronic exposure to inorganic arsenic in drinking water. Based on our structural data, it is tempting to speculate that this compound may, therefore, interact with serine hydrolases *in vivo*. Whether or not this interaction accounts mechanistically for any of the toxic effects of arsenic requires further study. However, the relatively high K_i for dimethylarsinic acid would suggest that the compound would only interfere with normal serine hydrolase function at sufficiently high concentrations of arsenic.

Acknowledgments—We thank the Stanford Synchrotron Radiation Laboratory. We are also grateful to Xiaoping Dai for assistance on synchrotron trips and Andreas Heine, Donmienne Leung, Benjamin F. Cravatt, Chi-Huey Wong, and Richard A. Lerner for helpful discussions. We also thank Ben List for generous use of his UV plate reader.

REFERENCES

1. Cameron, G. W., Jordan, K. N., Holt, P-J., Baker, P. B., Lowe, C. R., and Bruce, N. C. (1994) *Appl. Environ. Microbiol.* **60,** 3881–3883
2. Holt, P. J., Bruce, N. C., and Lowe, C. R. (1996) *Anal. Chem.* **68,** 1877–1882
3. Freedman, L. D., and Doak, G. O. (1955) *J. Am. Chem. Soc.* **77,** 6374–6376
4. Glazer, A. N. (1968) *J. Biol. Chem.* **243,** 3693–3701
5. Thomas, D. J., Styblo, M., and Lin, S. (2001) *Toxicol. Appl. Pharmacol.* **176,** 127–144
6. Maignan, S., Guilloteau, J. P., Zhou-Liu, Q., Clement-Mella, C., and Mikol, V. (1998) *J. Mol. Biol.* **282,** 359–368
7. Studier, F. W., and Moffatt, B. A. (1986) *J. Mol. Biol.* **189,** 113–130
8. Otwinowski, Z., and Minor, W. (1997) *Methods Enzymol.* **276,** 307–326
9. Terwilliger, T. C., and Berendzen, J. (1997) *Acta Crystallogr. Sec. D***53,** 571–579
10. Terwilliger, T. C. (2000) *Acta Crystallogr. Sec. D* **56,** 965–972
11. Lamzin, V. S., and Wilson, K. S. (1993) *Acta Crystallogr. Sec. D* **49,** 129–149
12. Jones, T. A., Zou, J. Y., Cowan, S. W., and Kjeldgaard, M. (1991) *Acta Crystallogr. Sec. A* **47,** 110–119
13. Brünger, A. T., Adams, P. D., Clore, G. M., Delano, W. L., Gros, P., Grosse-Kunstleve, R. W., Jiang, J.-S., Kuszewski, J., Nilges, M., Pannu, N. S., Read, R. J., Rice, L. M., Simonson, T., and Warren, G. L. (1998) *Acta Crystallogr. Sec. D* **54,** 905–921
14. Sheldrick, G. M., and Schneider, T. R. (1997) *Methods Enzymol.* **277,** 319–343
15. Wei, Y., Contreras, J. A., Sheffield, P., Osterlund, T., Derewenda, U., Kneusel, R. E., Matern, U., Holm, C., and Derewenda, Z. S. (1999) *Nat. Struct. Biol.* **6,** 340–345
16. De Simone, G., Galdiero, S., Manco, G., Lang, D., Rossi, M., and Pedone, C. (2000) *J. Mol. Biol.* **303,** 761–771
17. De Simone, G., Menchise, V., Manco, G., Mandrich, L., Sorrentino, N., Lang, D., Rossi, M., and Pedone, C. (2001) *J. Mol. Biol.* **314,** 507–518
18. Nardini, M., and Dijkstra, B. W. (1999) *Curr. Opin. Struct. Biol.* **9,** 732–737
19. Heikinheimo, P., Goldman, A., Jeffries, C., and Ollis, D. (1999) *Structure* (*Lond.*) **7,** 141–146
20. Connolly, M. L. (1983) *J. Appl. Crystallogr.* **16,** 548–558
21. Sheriff, S., Hendrickson, W. A., and Smith, J. L. (1987) *J. Mol. Biol.* **197,** 273–296
22. Stanfield, R. L., Takimoto-Kamimura, M., Rini, J. M., Profy, A. T., and Wilson, I. A. (1993) *Structure* (*Lond.*) **1,** 83–93
23. Sussman, J. L., Harel, M., Frolow, F., Oefner, C., Goldman, A., Toker, L., and Silman, I. (1991) *Science* **253,** 872–879
24. Allen, F. H., and Kennard, O. (1993) *Chem. Design Automation News* **8,** 31–37
25. Longhi, S., Nicolas, A., Creveld, L., Egmond, M., Verrips, C. T., de Vlieg, J., Martinez, C., and Cambillau, C. (1996) *Proteins* **26,** 442–458
26. Millard, C. B., Kryger, G., Ordentlich, A., Greenblatt, H. M., Harel, M., Raves, M. L., Segall, Y., Barak, D., Shafferman, A., Silman, I., and Sussman, J. L. (1999) *Biochemistry* **38,** 7032–7039
27. Ghosh, D., Sawicki, M., Lala, P., Erman, M., Pangborn, W., Eyzaguirre, J., Gutierrez, R., Jornvall, H., and Thiel, D. J. (2001) *J. Biol. Chem.* **276,** 11159–11166
28. Holm, L., and Sander, C. (1993) *J. Mol. Biol.* **233,** 123–138
29. Harel, M., Quinn, D. M., Nair, H. K., Silman, I., and Sussman, J. L. (1996) *J. Am. Chem. Soc.* **118,** 2340–2346
30. Jaeger, K. E., Dijkstra, B. W., and Reetz, M. T. (1999) *Annu. Rev. Microbiol.* **53,** 315–351
31. Kraut, J. (1977) *Annu. Rev. Biochem.* **46,** 331–358
32. Pindel, E. V., Kedishvili, N. Y., Abraham, T. L., Brzezinski, M. R., Zhang, J., Dean, R. A., and Bosron, W. F. (1997) *J. Biol. Chem.* **272,** 14769–14775
33. Esnouf, R. M. (1999) *Acta Crystallogr. Sec. D* **55,** 938–940
34. Merritt, E. A., and Murphy, M. E. P. (1994) *Acta Crystallogr. Sec. D* **50,** 869–873
35. Westhead, D. R., Slidel, T. W. F., Flores, T. P. J., and Thornton, J. M. (1999) *Protein Sci.* **8,** 8897–8904